Vibrational spectroscopy for discrimination and quantification of clinical chemotherapeutic preparations

Alaa A. Makki [a, b], Victor Massot [c], Hugh J. Byrne [f], Renaud Respaud [d], Dominique Bertrand [e], Elhadi Mohammed [b], Igor Chourpa [a], Franck Bonnier [a,*]

[a] Université de Tours, EA 6295 Nanomédicaments et Nanosondes, 31 avenue Monge, 37200 Tours, France

[b] Faculty of Pharmacy, University of Gezira, P.O. Box 20, 21111 Wad Madani, Sudan

[c] Unité de Biopharmacie Clinique Oncologique, Pharmacie, CHU de Tours, France

[d] Université de Tours, UMR 1100, CHRU de Tours, Service de Pharmacie, F-37032 Tours, France

[e] Data_Frame, 25 rue Stendhal, 44300 Nantes, France

[f] FOCAS Research Institute, TU Dublin, City Campus, Kevin Street, Dublin 8, Ireland

Abstract

In a clinical setting, analytical quality control of the administration of chemotherapeutic preparations is required to ensure patient safety with respect to the dose and more importantly the correct anticancer drug. As such, analytical tools enabling both qualitative and quantitative verification of the composition of prepared solutions can greatly benefit the hospital workflow, reducing cost and ultimately ensuring optimum patient care and outcome. Raman and infrared spectroscopy are rapid and cost-effective techniques, delivering label free molecular characterisation of samples. A comparative study has been conducted using four commercial intravenous formulations, DOXORUBICINE TEVA®, CERUBIDINE®, HOLOXAN® and METHOTREXATE MYLAN®, respectively containing doxorubicin, daunorubicin, ifosfamide and methotrexate as active drugs. Using clinically relevant concentration ranges prepared in 0.9% NaCl or 5% glucose solutions, it is demonstrated that 100% discrimination can be achieved for all formulations using either Raman or IR spectroscopic techniques, combined with multivariate discriminant analysis. Employing a partial least square regression analysis, Raman spectroscopy performed on liquid samples delivers a better accuracy compared to infrared, based on the mean squared error of cross validation. However, it is demonstrated that, despite the strong contribution of glucose and mannitol, an excipient found in CERUBIDINE®, infrared spectroscopy remains an equally viable option for translation into clinics.

Key words: ATR-FTIR spectroscopy, Raman spectroscopy, chemotherapeutics, Chemometrics, Partial least squares regression.

1. Introduction:

Chemotherapeutic drugs remain one of the main treatments for cancer, although they can result in serious side effects, due to the non-selective targeting of both cancer and healthy cells, and toxicity to patients is a major concern (1,2). Nowadays, individualised doses, in the form of solutions of commercial formulations, are prescribed to minimise adverse effects to patients while aiming to administer chemotherapeutic drugs within a sometimes-narrow therapeutic window. The safety for patients is strongly dependent on the precise preparation and administration of the chemotherapeutic solutions, i.e. the correct drug administered at the prescribed dose. Therefore, analytical quality control (AQC), i.e. identification and quantification of active drugs, before the solutions are released from the preparation units to the patient's bedside for administration has become a crucial step in the clinical workflow, and intravenous chemotherapeutic solutions are systematically analysed and approved to prevent discrepancies between prescription and administration. Although practices vary in different hospitals, the identification of the active pharmaceutical ingredients (APIs) should be achieved with 100% accuracy, while the tolerance for errors between targeted and estimated concentrations can be as high as 10% (3).

There is, however, no universally accepted or agreed protocol for AQC of prepared solutions and a diverse range of analytical techniques are used in the hospital setting for this purpose, including high-performance liquid chromatography (HPLC) or flow injection analysis (FIA), generally coupled to UV detection, or more elaborated techniques such as mass spectrometry (MS). HPLC remains the gold standard for quality control (4,5), while MS plays a rather crucial role during the drug discovery and development process, for chemotherapeutic characterisation (6–8) or for therapeutic drug monitoring (TDM), which requires quantification of low concentration of drugs within biological matrices such as serum (9). Considering the huge number of solutions which have to be analysed every single day, in addition to the analytical performance of the techniques, other criteria such as the need for sample preparation, time/material consumption, cost and staff requirements are considered prior to selection of an appropriate technique. Reducing the costs and the pressure on the workflow while preserving the reliability of the analytical protocols is a challenge.

Vibrational spectroscopic techniques, Raman scattering (RS) and infrared (IR) absorption, are structure-specific methods that can provide a molecular fingerprint for both qualitative and

quantitative analysis of solutions (10). They are non-destructive, label-free methods, that have gained recognition for clinical applications and quality control due to the minimal requirement for sample preparation and short analysis time (11). Vibrational spectroscopy has previously been explored in hospital settings in the context of AQC, which is performed before releasing the therapeutic prescriptions for administration (12–17). An instrument combining UV-visible and IR absorption techniques (Multispec ®, Microdom) has been proposed to perform analysis on chemotherapeutic solutions (18). However, the appropriateness of such a set up to fully exploit the coupling of those two methods is quite limited in aqueous solutions, since infrared suffers from the strong water absorbance (19). More recently, based on the fact that water is a relatively weak Raman scatter, the coupling of UV-visible absorption and Raman spectroscopy has emerged as a strong candidate for analysis of aqueous solutions (3,20).

Surprisingly, the literature reporting IR absorption and Raman spectroscopic analysis of chemotherapeutic solutions is limited (21–23). Although some relevant pharma-based publications can be found, none propose an in depth understanding of the origin of the spectra collected. A direct comparison between IR and Raman spectroscopy was performed by Makki *et al.,*(24) for the case of doxorubicin, epirubicin and daunorubicin in aqueous solutions. However, intravenous chemotherapeutic solutions are either prepared in the presence of 0.9% NaCl or 5% glucose (22,25,26), which potentially impact the signatures of the collected spectra. Therefore, the present study investigates the identification/discrimination and quantification of therapeutic solutions of four chemotherapeutic drugs (doxorubicin, daunorubicin, ifosfamide and methotrexate) by means of Attenuated Total Reflectance Infrared spectroscopy (ATR-IR) and Raman spectroscopy. In addition, to describe the vibrational characteristics of the drug molecule, the study assesses the possible matrix effect linked to either 0.9% NaCl or 5% glucose, for the drug solutions prepared at various concentrations corresponding to their respective therapeutic range.

2. Materials and Methods:

2.1 Anticancer drugs and sample preparation:

Four commercial formulations have been provided through a collaboration established with the University Hospital of Tours. More precisely, the UBCO unit (Unité de Biopharmacie Clinique Oncologique, Tours, France) deals with the preparation of individualised chemotherapeutic doses directly on site for rapid administration to patients.

DOXORUBICINE TEVA® (doxorubicin, injectable solution, 2 $g \cdot L^{-1}$ with HCl and NaOH (<1%) as excipients), and CERUBIDINE® (daunorubicin, lyophilised powder, 20 % w/w in mannitol), are anthracyclines which inhibit DNA and RNA synthesis (27), and are used in the treatment of breast cancer, lymphomas and multiple myelomas, lung cancer (28,29), Hodgkin's lymphomas, bladder lymphomas, soft tissues sarcomas, lung and testicular cancers (30).

HOLOXAN® (ifosfamide, 1000 mg powder for solution) is an oxazophosphorine alkylating drug, which induces DNA cross linking (31), used in the treatment of non-Hodgkin lymphomas, bone and soft tissues sarcomas (32). For HOLOXAN®, no excipients are listed by the manufacturers.

METHOTREXATE MYLAN® (methotrexate injectable solution 100 $g \cdot L^{-1}$ with NaCl as excipient) is an antifolate, which inhibits folic acid synthesis and is widely used to treat osteosarcomas, lymphomas, solid tumours, psoriasis, rheumatoid arthritis (33), head and neck cancer (34), breast cancer (35), acute lymphocytic leukaemia (36) and central nervous system lymphomas (37).

Based on records for recently prepared solutions at the UBCO unit, relevant therapeutic concentration ranges were established for the study. Sets of 10 solutions of each were prepared using serial dilutions in either 0.9% sodium chloride or 5% glucose (Table 1). 3 independent sets of samples were prepared from the stock solution for a total of 30 samples per drug. All samples were prepared freshly on the day of analysis and stored at 4°C in a dark room to avoid photo-damaging prior to spectral analysis.

For clarity, throughout the manuscript, commercial formulas are identified using their brand names DOXORUBICINE TEVA®, CERUBIDINE®, HOLOXAN®, METHOTREXATE MYLAN® while doxorubicin, daunorubicin, ifosfamide and methotrexate solely refer to the active drugs themselves.

Table 1. Concentration range for the 4 drugs analysed

Brand	Drug	Concentration range analysed (n = 10)
TEVA®	Doxorubicin	0.10 $g{\cdot}L^{-1}$ - 1.45 $g{\cdot}L^{-1}$
CERUBIDINE®	Daunorubicin	1.1 $g{\cdot}L^{-1}$ - 2 $g{\cdot}L^{-1}$
HOLOXAN®	Ifosfamide	2 $g{\cdot}L^{-1}$ - 17.75 $g{\cdot}L^{-1}$
MYLAN®	Methotrexate	3 $g{\cdot}L^{-1}$ – 21 $g{\cdot}L^{-1}$

1.2.1 Raman spectroscopic analysis

Raman spectra were collected using a Labram spectrometer (Horiba Jobin-Yvon, France) equipped with a 690 nm laser source. The set up was adapted to perform macroanalysis from solutions in quartz cuvettes. A macro-cuvette holder (Horiba Jobin-Yvon, France), was attached to the turret of the microscope, redirecting the laser through the samples with a 45° incidence mirror, allowing the micro spectrometer to be operated in a similar way to a UV/Vis benchtop spectrophotometer, sliding in and out the cuvettes between measurements. Using such a set up ensures maximum reproducibility during data collection without the requirement to readjust the laser focus between measurements, while enabling analysis of a large volume of solutions. 500 µL of the solution were placed in a quartz cuvette. The spectral range was set between 150 and 3750 cm^{-1}, with a spectral resolution of ~3 cm^{-1}, achieved using a 300 lines/mm grating. Two accumulations of 20 seconds were taken for each spectrum. 9 spectra were collected from each sample, 27 per concentration, and thus 270 for each drug analysed for each matrix, i.e. 0.9% NaCl and 5% glucose.

1.2.2 Infrared spectroscopic analysis

Infrared spectra were recorded with a Frontier, Fourier Transform IR (FTIR) spectrometer (Perkin Elmer, France) equipped with a multi-reflection diamond (n = 10) ATR accessory (ConcentratIR2™, Eurolabo, France). A drop of 2 µL was deposited directly on the ATR crystal and allowed to air dry prior to analysis. A background was acquired (4 scans) and ratioed with the sample spectra by the acquisition software (Spectrum, Perkin Elmer). Each IR spectrum resulted from 4 co-averaged scans collected over the range 600 – 4000 cm^{-1} with a spectral resolution of 2 cm^{-1}. 9 spectra were collected from each sample, 27 per

concentration. Thus, 270 spectra were collected for each drug analysed for each matrix, i.e. 0.9% NaCl and 5% glucose.

2.2.3 Data handling:

Raman and IR data sets have been pre-processed and analysed using MATLAB (Mathworks, USA).

a) Discriminant analysis: For the purpose of discriminative analysis, Raman and FTIR spectra were subjected to background correction by Extended Multiplicative Scattering Correction (EMSC) (38–40), in the range 300 – 3750 cm^{-1} for Raman spectra, whereas for ATR-FTIR spectra the range was 600 – 4000 cm^{-1}, followed by Lieber baseline correction (41–43) and vector normalisation (44) to minimise interferences from backgrounds (45). Pre-processed Raman and IR spectra were analysed in the fingerprint region of 600 – 1800 cm^{-1} by Partial Least Squares Discriminant Analysis (PLSDA), which is a well-established and widely used supervised classification method (22,46).While multivariate approaches such as PCA (Principal Components Analysis) provide valuable insights to the source of variance within datasets by reducing dimensionality to reveal underlying patterns, the interpretability of the analysis is directly linked to the complexity of the date set (i.e. number of samples), and it has been demonstrated the most specific analysis is obtained for pair wise system (47). Presently, the data set includes 80 groups (4 drugs, 2 matrices 0.9% NaCl and 5% glucose, of 10 systematically varied concentrations). PCA cannot readily be applied to differentiate all samples (data not shown), and moreover cannot provide a quantitative discriminative analysis. PLS-DA has been increasingly used over the last two decades to solve classification and discrimination problems of spectroscopic data (48). This supervised approach, like other discriminant analysis, requires knowledge of the class of each sample to construct a training set. Presently, PLSDA was used to discriminate between the 4 tested chemotherapeutic drugs in the 2 different matrices used for preparation of solutions. In order to avoid overoptimistic outcomes, it is recommended to perform the analysis between independent sets of data. 3 sets of 10 concentrations, Set 01, Set 02 and Set 03, have been recorded for each drug. For the discriminant analysis, the combination Set 1 and Set 2 were used as training sets (n = 40) for the construction of the model, while Set 03 was used solely as the test set (blind samples, n = 20). Therefore calibration, validation and test sets are kept independent. The optimal number of latent variables was selected with the validation set while the outcome of the PLSDA represents the classification of samples from the test set. Ultimately, the results were

presented in the form of confusion matrices, allowing calculation of the specificity and sensitivity of the discrimination achieved for the test set.

b) Quantitative analysis:

For the purpose of quantitative analysis, data were subjected to background correction by EMSC. No normalisation was applied, to maintain the linear relationship between spectral signal and concentration. Partial Least Squares Regression (PLSR) was applied to extract the quantitative information from data sets in the fingerprint region of 600 – 1800 cm^{-1}. Similar to PLSDA, Set 01 and Set 02 were used as training sets (n = 40) while Set 03 was used as the test set (n = 20). The 40 samples of the training set were further separated in the calibration and validation sets. For the purpose of quantitative analysis, 2/3 of samples were randomly selected as the calibration set and the remaining 1/3 were used as validation set. A 100-fold iteration was implemented to evaluate the robustness of the analysis with multiple random combinations of calibration/validation sets. However, the models were always tested with Set 03, used as unknown samples to be determined. The output of the PLSR analysis was evaluated using the Coefficient of Determination (R^2), and the Root Mean Square Error of Prediction (RMSEP) calculated from the test set (i.e. Set 03). The number of latent variables (LVs) was selected using the plot of Root Mean Square Error of Cross Validation (RMSECV), to preserve independency between training and test sets. The regression coefficients were also used to elucidate the spectral variables (wavenumbers) which contribute prominently to the regression models.

3. Results and discussions

3.1. Spectral characterisation of formulations

3.1.1. Raman analysis of commercial formulations

Figure 1 presents the chemical structures of doxorubicin, daunorubicin, ifosfamide and methotrexate, while Figure 2A shows the fingerprint region of corresponding Raman spectra obtained from their commercial stock solutions (DOXORUBICINE TEVA®, CERUBIDINE®, HOLOXAN® and METHOTREXATE MYLAN®, respectively). The Raman spectra recorded from distilled water and from relevant solutions of mannitol, glucose and 0.9% NaCl are displayed in Figure 2B. As expected, only 1% mannitol (spectrum a) and

5% glucose (spectrum b) solutions show some additional bands to those of water, while NaCl in solution is dissolved into its constituent ions and thus does not exhibit any vibrations.

Doxorubicin and daunorubicin are anthracyclines composed of a tetracycline ring, the aromatic moiety being linked by a glycosidic bond to daunosamine sugar (49–51) (Figure 1). Therefore, the fingerprint region of DOXORUBICINE TEVA® and CERUBIDINE® (Figure 2Aa and 2Ab) show strong Raman spectral features around 1100 cm^{-1} (aromatic C-H bending), between 1200-1250 cm^{-1} (C-O-H and in plane C-O stretching), 1300 cm^{-1} (C-O-H bending), 1450 cm^{-1} and 1580 cm^{-1} (aromatic ring stretching) and at 1650 cm^{-1} (stretching of H-bonded C=O group) (24). The chemical composition of the commercialised drug CERUBIDINE® differs from that of DOXORUBICINE TEVA® due to the presence of quite a high concentration of mannitol as excipient. Accordingly, in the Raman spectrum of CERUBIDINE®, a band originating from mannitol can be observed at 890 cm^{-1} (Figure 2B, spectrum a). The other bands of mannitol, expected at 798 cm^{-1}, 1276 cm^{-1}, 1309 cm^{-1} and 1468 cm^{-1} (Figure 2A, spectrum b), are overlapped by stronger Raman features from the aromatic chromophore of daunorubicin.

The chemical structure of ifosfamide (Figure 1) is comprised of chloroethyl groups attached to an endocyclic nitrogen (32,52). The main spectral characteristics of HOLOXAN® (Figure 2A, spectrum c) are thus observed at 668 cm^{-1} (ring bending), 791 cm^{-1} (C-Cl stretching), 1052 cm^{-1} (C-C aliphatic chain stretching), 1295 cm^{-1} (ring stretching), 1452 cm^{-1} (N-H bending), 1484 cm^{-1} (CH_2 scissoring) and 1649 (CH_2 deformation) (53,54). METHOTREXATE MYLAN® (methotrexate) spectrum is characterised by strong features at 1209 cm^{-1}, 1352 cm^{-1} and 1554 cm^{-1} and 1606 cm^{-1} assignable respectively to CH_2 wagging, aromatic C-C stretching and C-N stretching (Figure 2Ad). Other weaker bands are observed at 673 cm^{-1} (aromatic C-C-C in plane bending), 700 cm^{-1} (C-C in plane bending), 765 cm^{-1} (C-C out of plane bending) and 1292 cm^{-1} (-CH_3 symmetric deformation) (55). For both HOLOXAN® and METHOTREXATE MYLAN®, excipients present are either HCl or NaOH, which are not expected to present spectral features contributing in the Raman spectra in this range. Therefore, the peaks observed can be specifically attributed to the active drugs in solution.

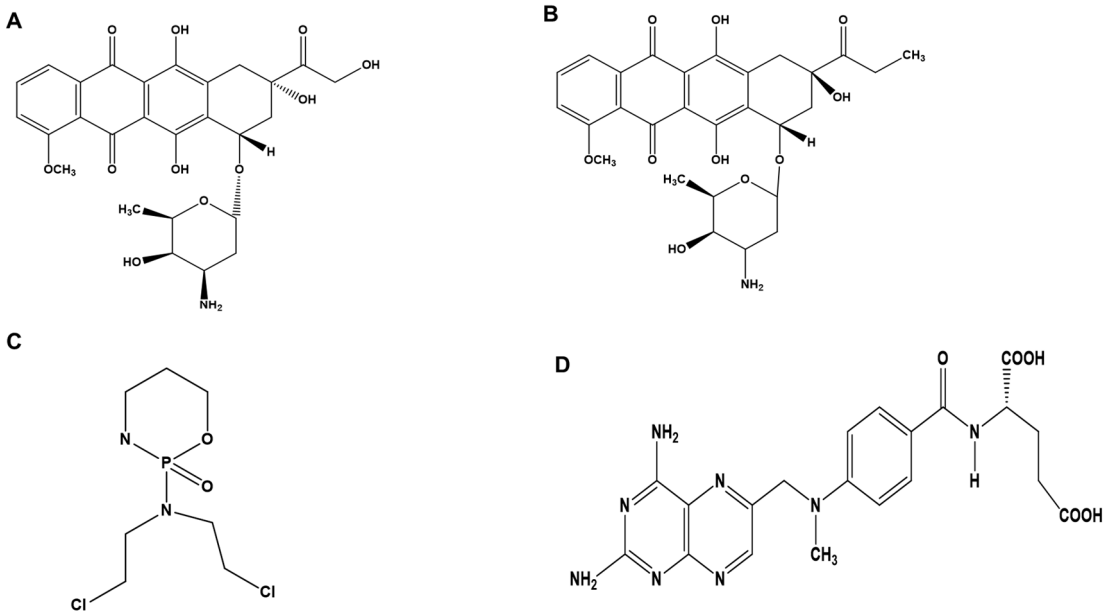

Figure 1: *chemical structures of A) Doxorubicin, B) Daunorubicin, C) Ifosfamide, D) Methotrexate.*

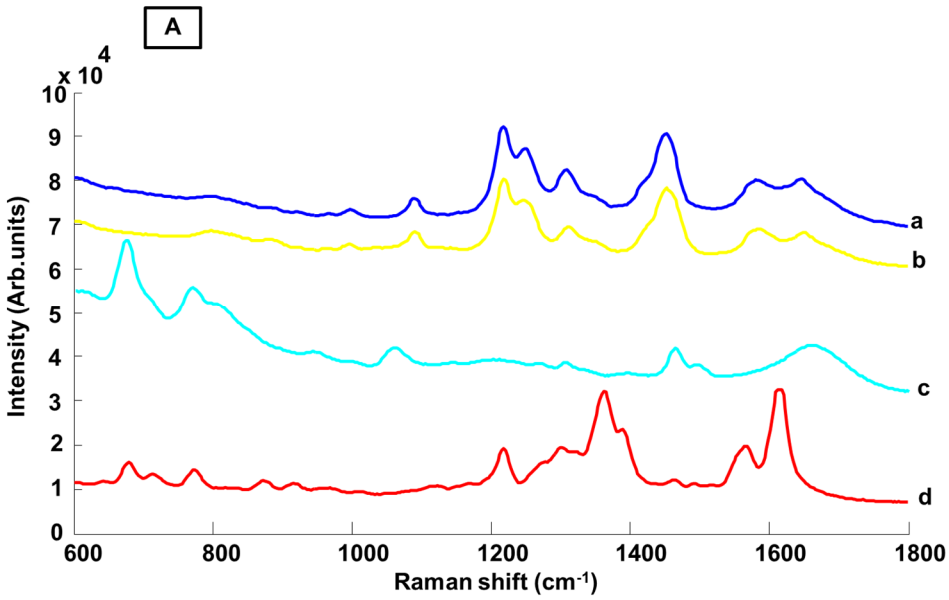

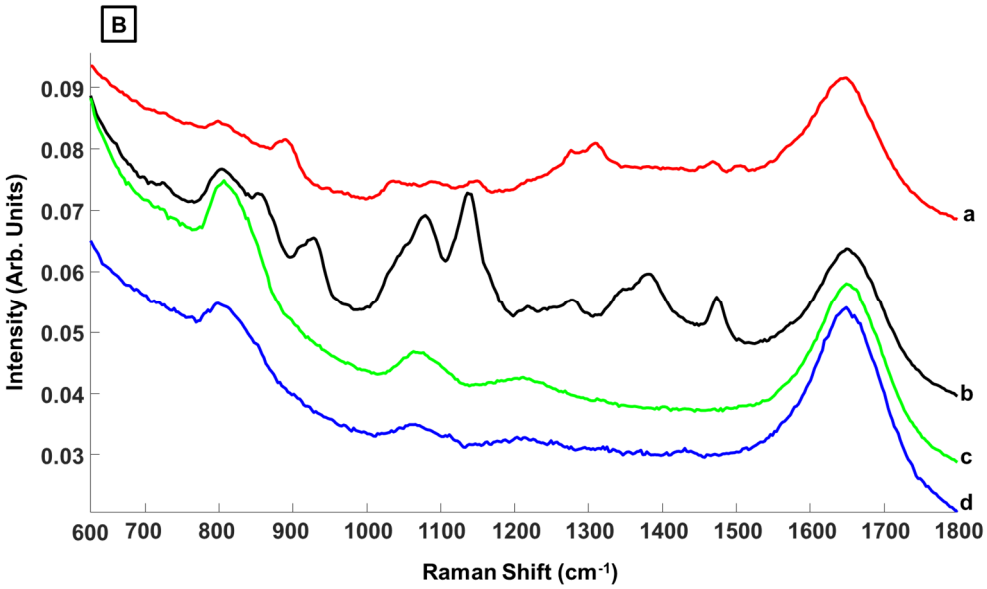

Figure 2: (A): Mean Raman spectra recorded from commercialised chemotherapeutics drug formula. DOXORUBICINE TEVA® 2 g·L^{-1} (a), CERUBIDINE® 2 g·L^{-1} (b), HOLOXAN® 40 g·L^{-1} (c) and METHOTREXATE MYLAN® 100 g·L^{-1} (d). (B): Mean Raman spectra recorded from Mannitol 1% (a), 5% glucose (b), 0.9% NaCl (c) and de-ionised water (d). Spectra are offset for clarity.

3.1.2. ATR-IR analysis of commercial formulations

In the ranges of concentrations used in this study, the strong water absorption at ~1640cm^{-1} dominates the IR spectrum of solutions, swamping characteristic features of the drugs (data not shown) and thus the only option was to record spectra from air dried drops deposited onto the ATR crystal for spectral characterisation. Figure 3A and Figure 3B presents ATR-FTIR spectra collected from the 4 drugs.

DOXORUBICINE TEVA® (Figure 3Aa) displays specific features at 1721 cm^{-1} (C=O stretching), 1616 cm^{-1} (N-H bending), 1576 cm^{-1} (ring breathing), 1444 cm^{-1} (-CH_3 bending), 1406 cm^{-1} (-CH_3 bending), 1210 cm^{-1} (C-C stretching), 1014 cm^{-1} (C-O (alcoholic) bending) and 987 cm^{-1} (C-O-H bending) (24). Mannitol presents a strong IR signature with a number of intense, sharp peaks across the 1800-600 cm^{-1} region (Figure 3Bb). As a consequence, numerous bands of the IR spectrum from CERUBIDINE® (Figure 3Ba) are attributed to features originating from this sugar. However, the strongest bands from CERUBIDINE® can be observed at 1712 cm^{-1} (C=O stretching), 1617 cm^{-1} (N-H bending), 1580 cm^{-1} (ring breathing), 1449 cm^{-1} (-CH_3 bending), 1139 cm^{-1} (ring breathing coupled with C-C=O bending), 1053 cm^{-1} (C-O (alcoholic) bending), 989 cm^{-1} (C-O-H bending), 966 cm^{-1} (-CH_3 rocking), 845 cm^{-1} (=C-H (aromatic) bending) and 818 cm^{-1} (N-H out of plane bending) (24).

The combined contribution of daunorubicin and mannitol bands implies some substantial differences between DOXORUBICINE TEVA® and CERUBIDINE®.

Considering the chemical structures of ifosfamide (Figure 1), it is not surprising that the infrared signature of HOLOXAN® greatly differs from that of the other drugs (Figure 3Ab), with strong bands at 1436 cm^{-1} (-CH_2 wagging), 1229 cm^{-1} (CH_2-Cl rocking), 1116 cm^{-1} (C-O bending), 1096 cm^{-1} (ring stretching), 1053 cm^{-1} (C-H wagging), 1030 cm^{-1} (C-C stretching), 973 cm^{-1} (ring stretching deformation), 925 cm^{-1} (C-O stretching), 876 cm^{-1} (ring stretching), 788 cm^{-1} (CH_2-Cl rocking) and 655 cm^{-1} (C-Cl stretching) (53,54). While the Raman spectrum of METHOTREXATE MYLAN® exhibits sharp, isolated intense peaks (Figure 3Ac), the ATR-IR spectrum has numerous overlapping bands resulting in broader features, notably in the range 1700-1200 cm^{-1}. However, specific peaks are found at 1587 cm^{-1} (C-C stretching), 1554 cm^{-1} (aromatic C-C stretching), 1506 cm^{-1} (C-N stretching), 1447 cm^{-1} (C-C stretching), 1398 cm^{-1} (CH_3 symmetric deformation), 1206 cm^{-1} (CH_2 wagging), 1097 cm^{-1} (CH_2 twisting) and 825 cm^{-1} (aromatic C-H out of plane bending) (55).

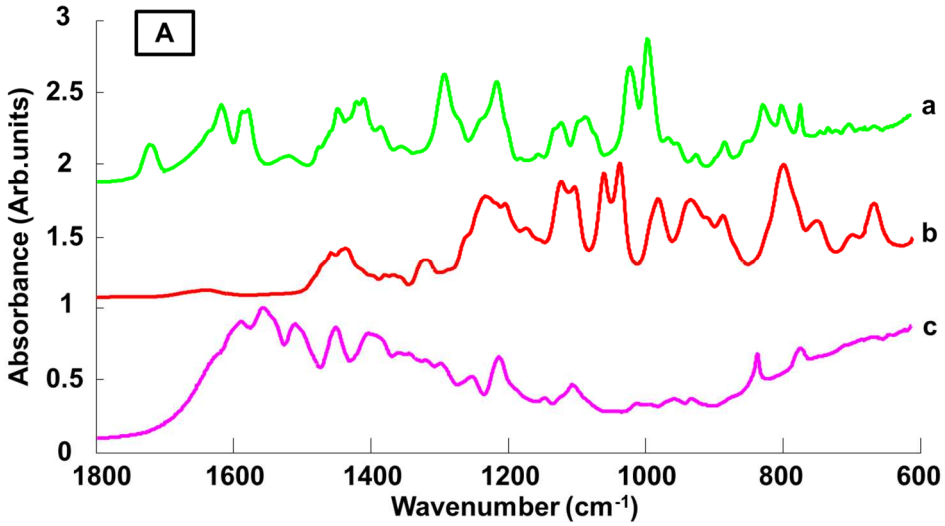

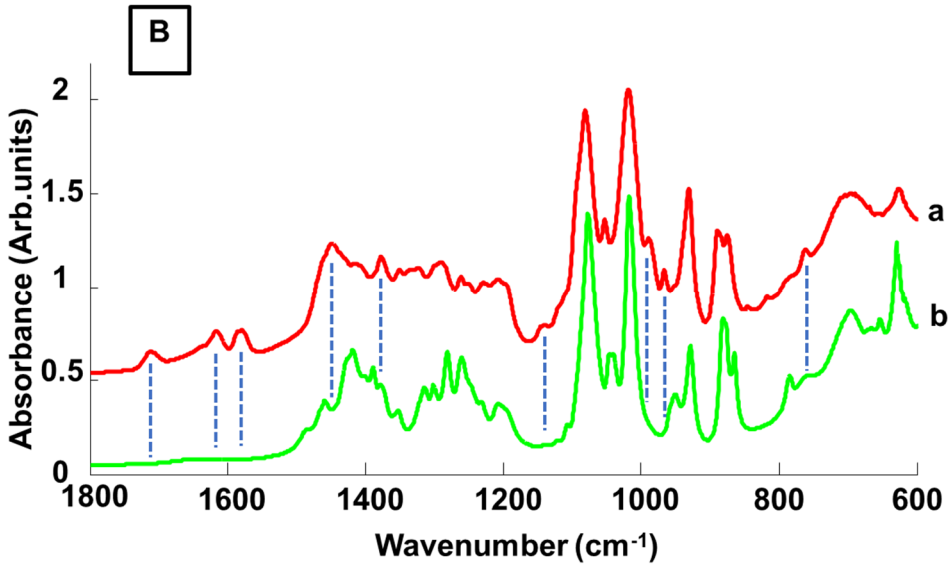

Figure 3: ***(A):*** *mean ATR-FTIR spectra recorded from commercial stock solutions. DOXORUBICINE TEVA® 2 g·L^{-1} (a), HOLOXAN® 40 g·L^{-1} (b) and METHOTREXATE MYLAN® 100 g·L^{-1} (c),* ***(B):*** *mean ATR-FTIR spectra recorded from CERUBIDINE® 2 g·L^{-1} (a) and mannitol 1% (b). Spectra are offset for clarity.*

3.2. Discriminant analysis using Raman and ATR-IR spectroscopy

Sensitivity and specificity are the main parameters used to determine the discriminative power of an analytical method. PLSDA was used to discriminate between the 4 tested chemotherapeutic drugs in the 2 different matrices used for preparation of solutions. For this purpose, samples of Set 01 and Set 02 have been used as the calibration and validation sets (n= 40) and Set 03 (n =20) was used a test set, i.e. as blind samples tested against the classification model constructed from the training sets. Therefore calibration, validation and test sets are kept independent. The optimal number of latent variables is selected with the validation set while the outcome of the PLSDA represents the classification of samples from the test set. Ultimately, the results were presented in the form of confusion matrices, allowing calculation of the specificity and sensitivity of the discrimination achieved for the test set. For Raman data, the discrimination was achieved using 5 latent variables (LVs) (as shown in Table 2). Ultimately, 100 % specificity and sensitivity were obtained.

Table 2. Specificity and sensitivity % of PLSDA calculated for the test set of Raman data using 5 LVs

Brand	0.9% NaCl		5% Glucose	
	Specificity	Sensitivity	Specificity	Sensitivity
TEVA®	100	100	100	100
CERUBIDINE®	100	100	100	100
HOLOXAN®	100	100	100	100
MYLAN®	100	100	100	100

Table 3 summarises the classification output for ATR-FTIR obtained with 11 LVs. Similar to Raman, 100% specificity and sensitivity are reached for the 4 tested chemotherapeutics drugs in either matrix. For both techniques, despite the structural similarities between doxorubicin and daunorubicin, as they belong to the anthracycline family of anticancer drugs and display structural similarities (56), PLSDA was able to differentiate between the DOXORUBICINE TEVA® and CERUBIDINE® formulations very clearly. This is in accordance with previous observations made by Makki *et al.,* (24), suggesting that the combination of structural differences and contribution of other formulation excipients provides sufficient spectral contrast to enable efficient discrimination.

Regression coefficients can be used to highlight the wavenumbers discriminating solutions prepared from the commercialised formulations. Figure 4 presents the regression coefficient resulting from the PLSDA applied to Raman spectra. The strong double bands between 1200-1250 cm^{-1} coupled to the strong feature at 1449 cm^{-1}, corresponding to DOXORUBICINE TEVA® and CERUBIDINE® are observed in the first regression coefficient (Figure 4a), whereas peaks identified in the first regression coefficient at 880 cm^{-1} and 1311 cm^{-1}, originating from mannitol, discriminate DOXORUBICINE TEVA® from CERUBIDINE®.

HOLOXAN® peaks can be identified at 680 cm^{-1} and 777 cm^{-1} in the first regression coefficient (Figure 4a). Peaks identifiable in the second regression coefficient (Figure 4b) at 673 cm^{-1}, 1216 cm^{-1}, 1360 cm^{-1}, 1561 cm^{-1} and 1607 cm^{-1} can be assigned to METHOTREXATE MYLAN®.

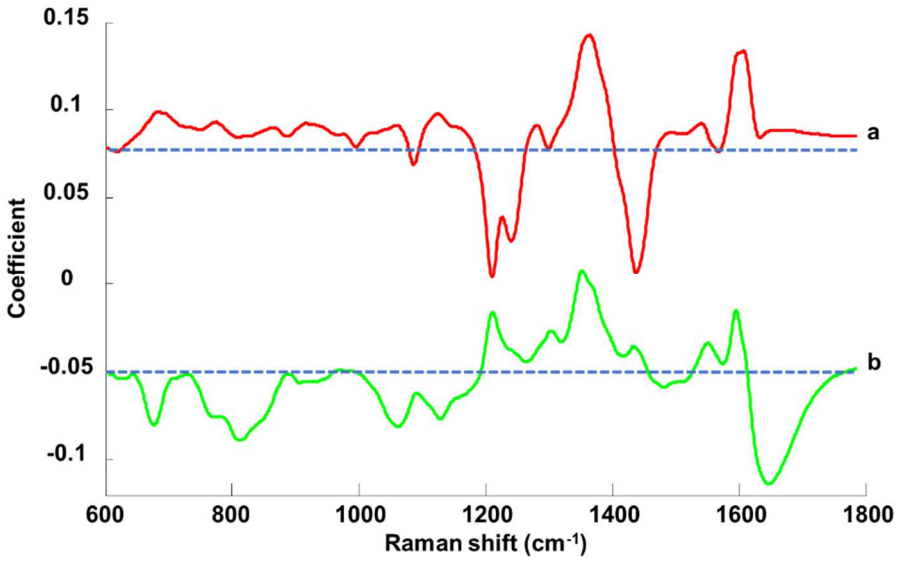

Figure 4: Regression coefficients a) 1 and b) 2 obtained from PLSDA analysis of Raman data. Offset for clarity, dot line indicates the zero.

In comparison, the contribution of glucose after air drying of samples is much more pronounced in ATR-FTIR spectra, and therefore the discrimination between solutions prepared in the two matrices can be easily achieved. This is highlighted by the first regression coefficient of PLSDA performed on IR spectra presented in Figure 5a, which displays pronounced features of glucose in the range 1000-1150 cm^{-1} (displayed in Figure 9). Moreover, as discussed in section 3.1.2, CERUBIDINE® ATR-FTIR spectra are strongly influenced by mannitol peaks, observed as the two main features between 1000-1100 cm^{1} in the 2^{nd} regression coefficient Figure 5b. Chemotherapeutic solutions also have specific additional features, as illustrated in Figure 3, and are therefore observed in both regression coefficients. For instance, the negative peaks in Figure 5a at 1587 cm^{-1}, 1554 cm^{-1}, 1506 cm^{-1}, 1447 cm^{-1}, 1206 cm^{-1}, 825 cm^{-1} correspond to specific peaks of METHOTREXATE MYLAN®, while the negative bands at 810 cm^{-1}, 788 cm^{-1}, 655 cm^{-1} and the quite specific double peaks at 1096 cm^{-1} and 1053 cm^{-1} can be assigned to HOLOXAN®.

Table 3. Specificity and sensitivity % of PLSDA calculated for the test set of ATR-FTIR data using 11 LVs

Brand	0.9% NaCl		5% Glucose	
	Specificity	Sensitivity	Specificity	Sensitivity
TEVA®	100	100	100	100
CERUBIDINE®	100	100	100	100
HOLOXAN®	100	100	100	100
MYLAN®	100	100	100	100

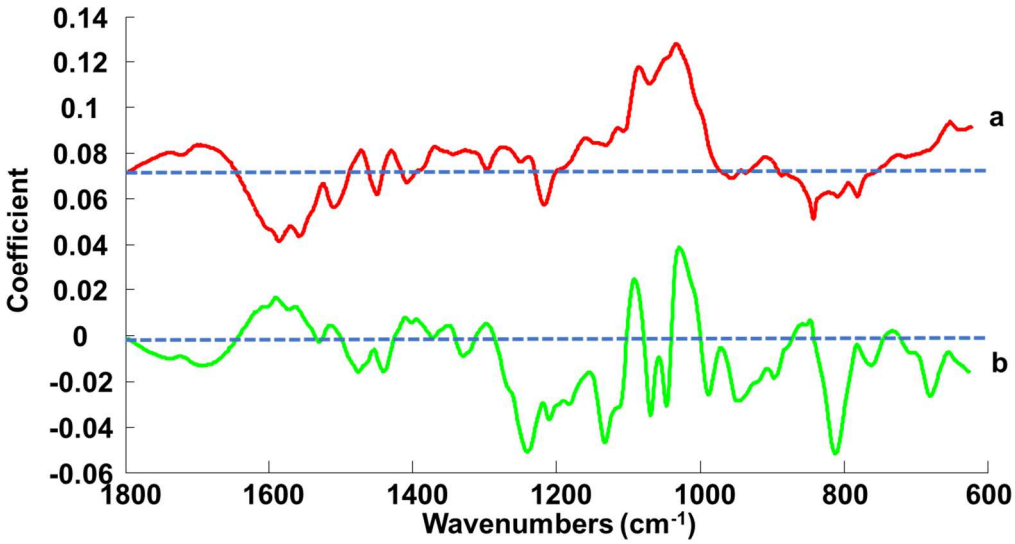

Figure 5: Regression coefficients, a) 1 and b) 2 obtained from PLSDA analysis on ATR-FTIR data. Offset for clarity, dot line indicates the zero.

3.3. Quantitative analysis of chemotherapeutics solutions

3.3.1. Raman spectroscopy

As an illustration of the quantitative potential of Raman spectroscopy, Figure 6 presents mean Raman spectra of the METHOTREXATE MYLAN® formula at different concentrations, from 21 to 3 $g \cdot L^{-1}$, all prepared in the presence of 5% glucose. Specific features at 1213 cm^{-1}, 1296 cm^{-1}, 1357 cm^{-1}, 1556 cm^{-1} and 1605 cm^{-1} are clearly identifiable and they naturally appear more pronounced as the drug concentration increases (Figure 6). Compared to those of the commercial sample, the band positions of the solutions prepared in glucose were only slightly affected (minor band shifts). Glucose displays only limited contributions identified at 927 cm^{-1}, 1079 cm^{-1} and 1136 cm^{-1} (Figure 2B, spectrum b).

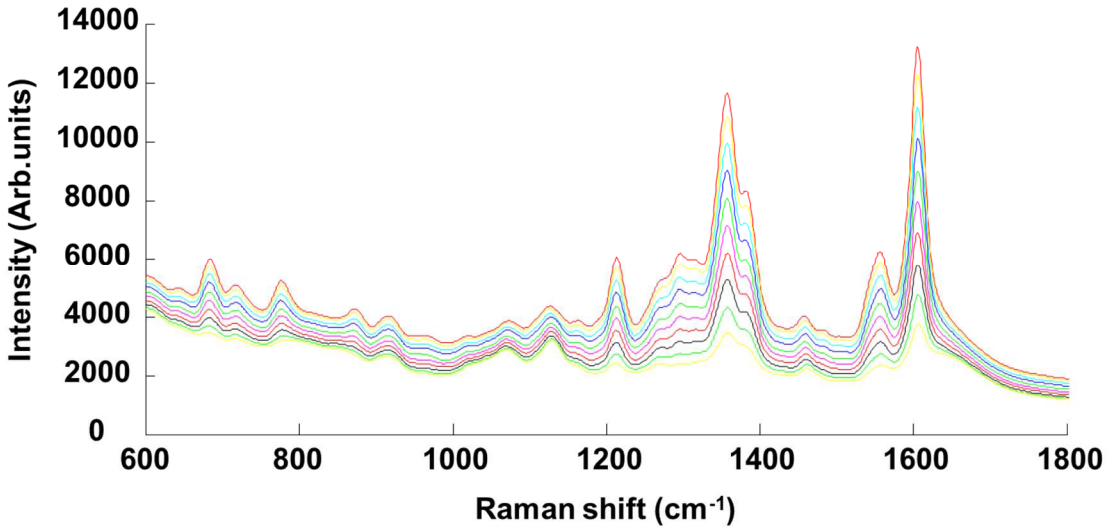

Figure 6: Mean Raman spectra of fingerprint regions of METHOTREXATE MYLAN® in 5% glucose solution following serial dilution. Spectra are organised as decreasing concentrations from the top to bottom, respectively corresponding to methotrexate concentrations of 21 g·L^{-1}, 19 g·L^{-1}, 17 g·L^{-1}, 15 g·L^{-1}, 13 g·L^{-1}, 11 g·L^{-1}, 9 g·L^{-1}, 7 g·L^{-1}, 5 g·L^{-1} and 3 g·L^{-1}.

In the present study, the approach for PLSR consisted of dividing the data into training and test sets. 2/3 of samples of the training set (n sample = 13) were identified as calibration and the remaining 1/3 (n sample = 7) were used as validation set. The samples from Set 03 were used independently and injected in the constructed quantitative model as bind samples. The RMSECV shows a marked decrease as a function of the number of LVs used in the PLSR model (Figure 7A). Above 3 LVs, there was no further statistical difference, indicating that only noise remained in the data and no further improvement in quantification could be achieved. The corresponding regression model presented in Figure 7B has been obtained from the test set. The error bars were calculated form the 100-fold iterations, indicating the reproducibility of the spectral collection using the macro set up. The R^2 value was found to be 0.9999 and the RMSEP was equal to 0.0448 g·L^{-1}, highlighting the quality of the fitting achieved and the accuracy of the predictive model. The mean standard deviation (STD) for the RMSEP was found to be 0.028 g·L^{-1}. The regression coefficient confirmed the predictive model was constructed based on METHOTREXATE MYLAN® features (Figure 7C). Notably, the presence of peaks at 1213 cm^{-1}, 1296 cm^{-1}, 1357 cm^{-1}, 1556 cm^{-1} and 1605 cm^{-1} confirmed the molecular specificity of the analysis has been preserved. Moreover, no prominent features of glucose are evident.

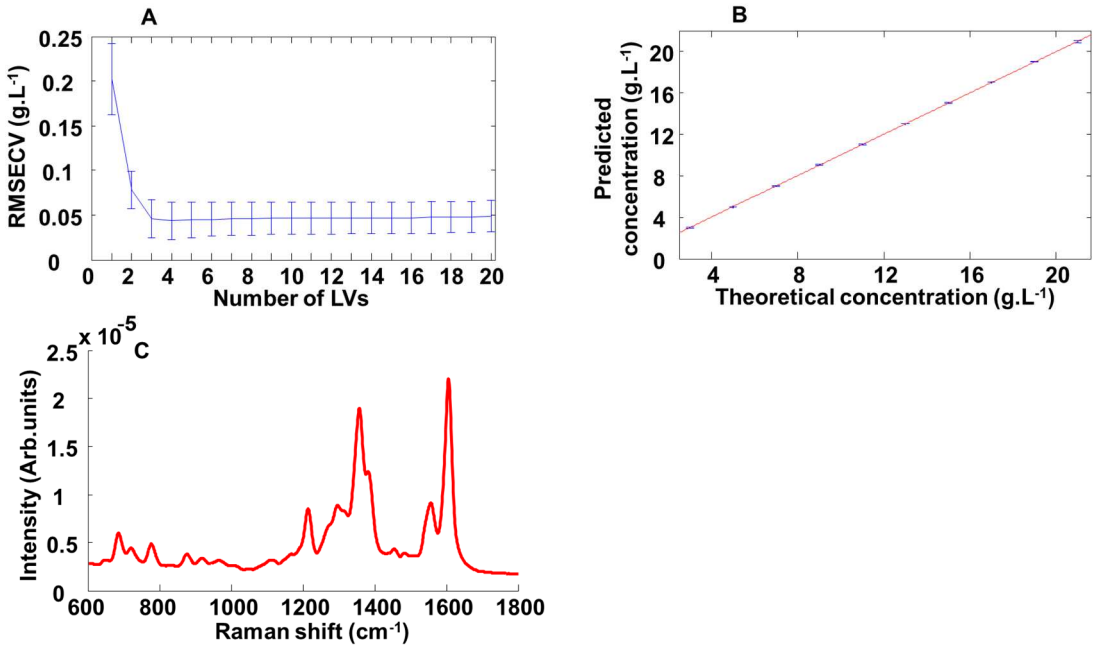

Figure 7: PLSR analysis performed on Raman spectra collected from METHOTREXATE MYLAN® solution in 5% glucose. A) RMSECV, B) Regression plot for the test set with 3 LVs and C) Regression coefficient.

Table 4 presents the PLSR results for all 4 commercial formulations, under the different conditions tested. For most of them, R^2 is close to, or equal to, 1 in both NaCl and glucose matrices. The lowest value of R^2 is found to be 0.9973 for CERUBIDINE®, in 0.9% NaCl. RMSEP values range from 0.0027 g·L^{-1} to 0.1759 g·L^{-1}, depending on the formulation and matrix used. To better appreciate the implication of the results, one could compare the RMSEP with the median concentration of the range used. For example, in the case of DOXORUBICINE TEVA® in 0.9% NaCl, the median concentration is 0.77 g·L^{-1}, and thus the RMSEP represents 0.6% of this value, suggesting the model is quite accurate. The highest RMSEP of 0.1759 g·L^{-1} is found for HOLOXAN® in 5% glucose, which only represents 1.8% of the median concentration. Therefore, it is observed that, overall, the RMSEP is relatively low compared to the range of concentrations analysed, indicating suitable sensitivity of Raman analysis for the chemotherapeutic solutions analysed, considering the clinical tolerance between the targeted concentration and the estimated concentration is 10%. As illustrated in Figure 1, the different commercial drug formulations do not have the same Raman response, and while METHOTREXATE MYLAN® has strong features, the signal collected from HOLOXAN® has much lower intensity. Figure 8 further illustrates the spectral variations in the range of concentrations analysed for HOLOXAN® in 5% glucose. One can

see that the underlying contribution from water (Figure 2Bd) and glucose (Figure 2Bb) are more prominent across the range of concentrations analysed, compared to the other solutions. Nevertheless, PLSR analysis enables accurate quantification.

Table 4. PLSR results obtained from the 4 chemotherapeutic drugs solutions tested in 2 matrices by Raman spectroscopy

Drug	Matrix	R^2	RMSEP	%RMSEP	LVs
TEVA®	0.9%NaCl	0.9999	0.0048	0.6	3
	5% glucose	1	0.0027	0.3	3
CERUBIDINE®	0.9%NaCl	0.9973	0.0152	0.9	4
	5% glucose	0.9994	0.0075	0.5	2
HOLOXAN®	0.9%NaCl	0.9995	0.1117	1.1	3
	5% glucose	0.9989	0.1759	1.8	4
MYLAN®	0.9%NaCl	1	0.0451	0.4	3
	5% glucose	0.9999	0.0448	0.4	3

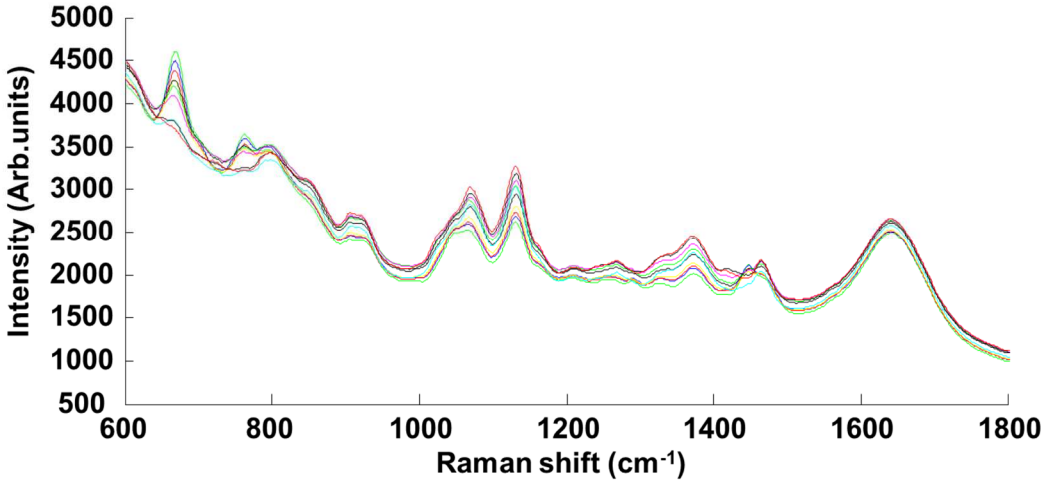

Figure 8: Mean Raman spectra of fingerprint regions of HOLOXAN® in 5% glucose solution following serial dilution. Spectra are organised as decreasing concentrations from the top to bottom, respectively corresponding to HOLOXAN® concentrations of 17.75 $g{\cdot}L^{-1}$, 16 $g{\cdot}L^{-1}$, 14.25$g{\cdot}L^{-1}$, 12.5 $g{\cdot}L^{-1}$, 10.75 $g{\cdot}L^{-1}$, 9 $g{\cdot}L^{-1}$, 7.25 $g{\cdot}L^{-1}$, 5.5 $g{\cdot}L^{-1}$, 3.75 $g{\cdot}L^{-1}$ and 2 $g{\cdot}L^{-1}$.

3.3.2. ATR-FTIR spectroscopy

Similar to Raman, the ATR-FTIR spectra have been subjected to PLSR to perform quantitative analysis. Glucose displays bands over the fingerprint range with main features found at 1420 cm^{-1}, 1358 cm^{-1}, 1315 cm^{-1}, 1258 cm^{-1}, 1145 cm^{-1}, 1100 cm^{-1}, 1071 cm^{-1}, 1020 cm^{-1}, 899 cm^{-1}, 842 cm^{-1} and 770 cm^{-1} (Figure 9A), while NaCl displays no significant spectral contribution (data not shown). Figure 9B illustrates, for the example of METHOTREXATE MYLAN®, how glucose has a strong contribution resulting in a spectral signature mixed with the drug features.

The RMSECV was used to determine the optimal number of latent variables while avoiding overfitting of results, as illustrated for METHOTREXATE MYLAN® in Figure 10A. The regression plot from the samples of the test set constructed with 5 LVs delivers an R^2 value of 0.9966 and RMSEP of 0.3492 $g{\cdot}L^{-1}$ (Figure 10B). The regression coefficient presented in Figure 10C exhibits features related to METHOTREXATE MYLAN® at 1589 cm^{-1}, 1558 cm^{-1}, 1511 cm^{-1}, 1451 cm^{-1}, 1394 cm^{-1}, 1338 cm^{-1}, 1292 cm^{-1}, 1247 cm^{-1}, 1208 cm^{-1}, 1139 cm^{-1}, 825 cm^{-1} and 760 cm^{-1} consistent with those identified as characteristic in Figure 3Ac. The regression coefficient also exhibits features from the glucose that are negative, indicating they are anti-correlated with METHOTREXATE MYLAN® concentrations.

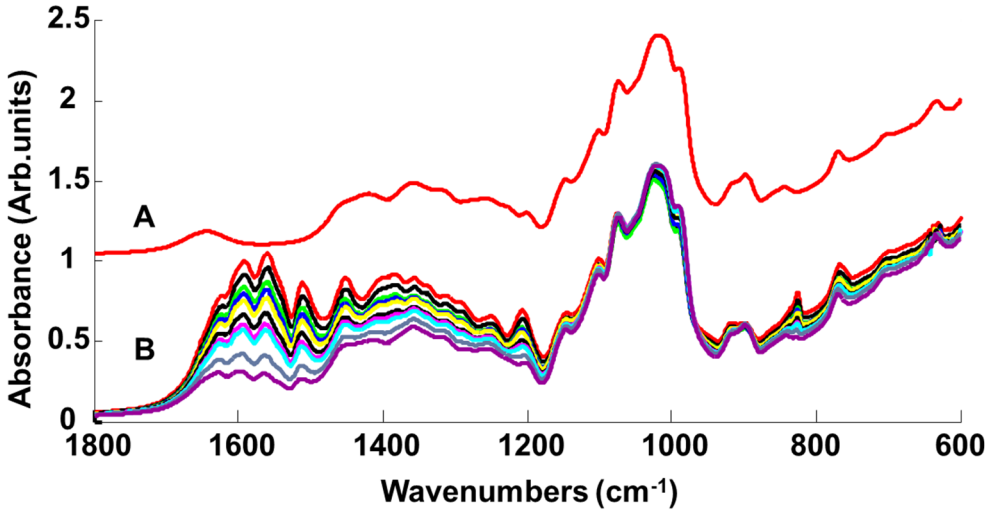

Figure 9: mean ATR-FTIR spectra of fingerprint regions of: A) 5% glucose and B) methotrexate in 5% glucose solution following serial dilution. METHOTREXATE MYLAN® spectra are organised as decreasing concentrations from the top to bottom, respectively corresponding to methotrexate concentrations of 21 $g{\cdot}L^{-1}$ (red), 19 $g{\cdot}L^{-1}$ (black), 17 $g{\cdot}L^{-1}$ (green), 15 $g{\cdot}L^{-1}$ (blue), 13 $g{\cdot}L^{-1}$ (yellow), 11 $g{\cdot}L^{-1}$ (black), 9 $g{\cdot}L^{-1}$ (magenta), 7 $g{\cdot}L^{-1}$ (cyan), 5 $g{\cdot}L^{-1}$ (grey) and 3 $g{\cdot}L^{-1}$ (purple). 5% glucose spectrum is offset for clarity.

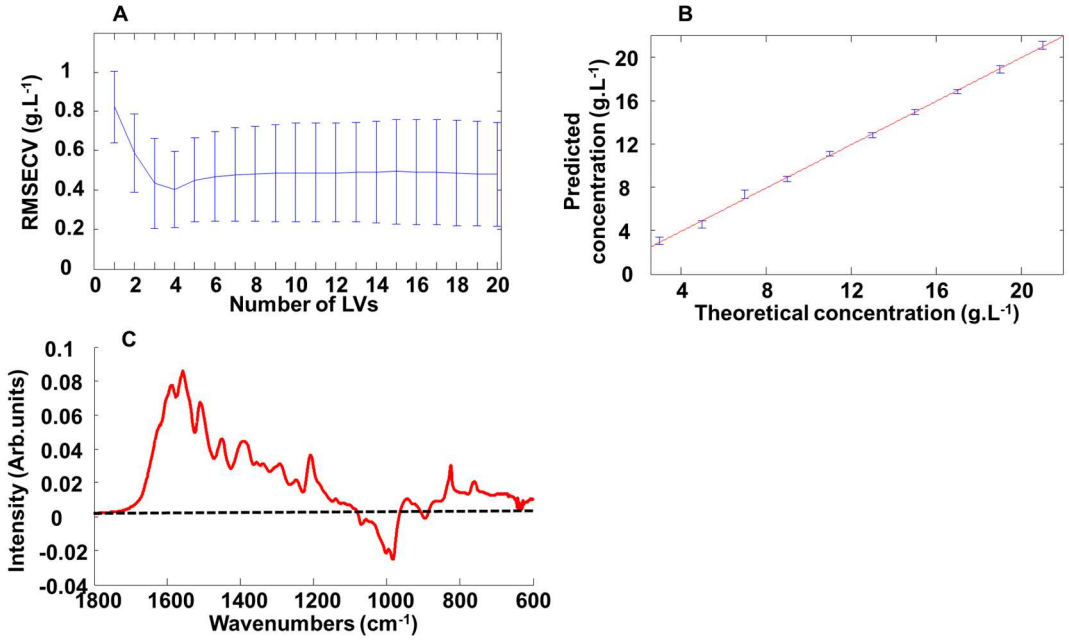

Figure 10: PLSR analysis performed on METHOTREXATE MYLAN® in 5% glucose solution tested by ATR-FTIR. A) RMSECV, B) Regression fitting for the test set obtained with 5 LVs and C) regression coefficient.

Table 5 summarises the PLSR results obtained for the four commercial drugs. Although the R^2 values are comparable to those observed with Raman analysis, the RMSEP are generally higher for ATR-FTIR, ranging from 0.018 g·L^{-1} and 0.8252 g·L^{-1}. Comparing the RMSEP to the median concentration of the range analysed for CERUBIDINE® in 0.9% NaCl (the lowest), represents value of 1.2% is obtained, while for METHOTREXATE MYLAN® in 0.9% NaCl (the highest) it increases to 6.9%. As a reminder, for Raman analysis, the highest value, for HALOXAN® in 5% glucose was found to be 1.8% of the median concentration (Table 4). Undoubtedly, the precision of analysis performed with ATR-FTIR is lower than that of Raman spectroscopy, most probably explained by the extra processing step of sample drying. It has been demonstrated that the linear, Lambert-Beer like relationship between measured absorbance and solution concentration is not well preserved in ATR-FTIR measurements of dried precipitates (57), and other effects such as spot size difference, variation in drop centring on the reduced diamond crystal surface and drying behaviour between drops could also contribute to the larger error of the ATR-FTIR analysis. Nevertheless, ATR-FTIR coupled to PLSR displays exhibits excellent performance for quantitative analysis, within the accepted clinical tolerance. Although glucose is a

particularly strong absorber in the infrared, within the respective relevant ranges of each drugs, specific features can be extracted and used for reliable regression models.

Table 5. PLSR results obtained from the 4 chemotherapeutic drugs solutions tested in 2 matrices by ATR-FTIR

Drug	Matrix	R^2	RMSEP	%RMSEP	LVs
TEVA®	0.9%NaCl	0.9983	0.0180	2.3	4
	5% glucose	0.9884	0.0489	6.3	6
CERUBIDINE®	0.9%NaCl	0.9964	0.0183	1.2	5
	5% glucose	0.9959	0.0184	1.2	6
HOLOXAN®	0.9%NaCl	0.9968	0.2829	2.9	6
	5% glucose	0.9953	0.3491	3.5	5
MYLAN®	0.9%NaCl	0.9811	0.8252	6.9	3
	5% glucose	0.9966	0.3492	2.9	5

4. Discussion

Analytical quality control is used to validate the conformity of chemotherapeutic solutions before release to a patient's bedside for injection represents a substantial economic burden as well as daily workload for hospitals. While sophisticated techniques such as liquid chromatography coupled to mass spectrometry could be deployed to ensure the safety of patients, time constraints and cost of analysis are limiting factors. Rapid, cost effective techniques with minimal sample preparation could contribute to speeding up the workflow. Vibrational spectroscopy enables direct molecular fingerprinting of samples to deliver quantification and discrimination of the chemotherapeutic solutions studied.

The first observation is that both Raman and ATR-FTIR are both affected by the type of matrix used, either NaCl 0.9% or 5% glucose. Glucose presents a number of specific features found in Raman and infrared spectra collected from chemotherapeutic solutions (Figure 6 and 9). However, it is observed that the glucose contribution is greater in infrared spectra, exhibiting more intense bands compared to the commercialised drugs solutions (see Figure 9b for MYALN®). This observation was consistent for the four solutions (data not shown). The relative contribution of glucose will differ depending on the strength of the spectral response collected from chemotherapeutic drugs. While, for Raman spectroscopy, molecules with conjugated rings are well known to be strong scatters, delivering intense Raman peaks

covering the glucose features (see example of METHOTREXATE MYLAN® for methotrexate, Figure 6), other chemical structures such as ifosfamide found in HOLOXAN® are considerably less Raman active. The Raman features from the chemotherapeutic solution are weaker (Figure 8), although the range of concentrations is close to that of METHOTREXATE MYLAN®, and consequently the glucose bands appear more prominent. The second observation is that, in both Raman and infrared, the samples are analysed as complex solutions with possible spectral contribution from all ingredients (i.e. excipients). For CERUBIDINE®, mannitol is present in the formulation at a concentration 5 times higher than daunorubicin itself. Similar, to glucose, mannitol is not a strong Raman scatterer and, as a result, its spectral features are not observed prominently in the Raman spectra of the chemotherapeutic solution (Figure 2Ab). However, sugars display strong absorbance in the IR, and, as a result, the spectra are dominated by mannitol features (Figure 3Ba).

Overall, both techniques enable quantitative and discriminative analysis. Glucose having a low contribution in spectra, it is not surprising to achieve 100% discrimination between the four chemotherapeutic solutions, although it is interesting to note that, for IR, the specificity of the analysis is preserved thanks to bands assigned to the drugs and/or excipients.

In terms of quantitative analysis, Raman is found to be slightly more accurate than IR, based on the values of RMSEP (Table 4 and Table 5). For DOXORUBICINE TEVA® in 5% glucose and METHOTREXATE MYLAN® in 0.9% NaCl, the RMSEP obtained was more than 5% of the median concentration of the range analysed by IR spectroscopy, while for Raman the highest was 1.8%.

The observations of the study lead directly to a discussion about the adaptivity of vibrational techniques. Raman microspectroscopy has benefitted from significant technological evolutions in recent decades (58–61). The systems are confocal thus potentially enabling analysis through packaging (62), and, notably, Spatially Offset Raman Spectroscopy is now being introduced in airport security screening to analyse suspicious items without opening containers (https://www.agilent.com/en/technology/spatially-offset-raman-spectroscopy). This is relevant for the safety of staff members performing AQC, as the ability to analyse the prescription without the requirement of extracting it from the infusion bag could reduce exposure to toxic compounds. Although early studies have investigated such applications of confocal Raman spectroscopy with inverted microscope setups or transportable devices (12,15), in recent years, few documented studies have supported the translation into clinics of non-invasive analysis. Considering the strength of spectral features and the concentrations used in treatments, it could be expected that exploitable data could be collected directly

through plastic layers, although extended investigations are required to confirm the accuracy and specificity. Secondly, manufacturers have devoted considerable efforts towards miniaturisation of the Raman spectroscopic systems, ranging from transportable (benchtop) apparatus equipped with deported probes to handheld systems. Recently Lee *et al.,* have reported demonstration of analytical performance of handheld systems to control anthracyclines (21) and taxanes (22). However, the experimental design used solutions contained in glass vials during the analysis, and therefore the results hardly demonstrate the feasibility to work directly in plastic bags. The exact analytical performance of non-invasive Raman has therefore yet to be established and validated.

In comparison, the main handicap for infrared spectroscopy in this context is the strong absorption of water. Although protocols for analysis of, for example protein secondary structure in the native aqueous environment have been described (63), optically thin cells, (of order <10 μm), with IR transparent windows are required, and relatively high concentration solutions (>3 mg/mL) are recommended, rendering the technique not so conducive to routine clinical analysis. The requirement for drying of samples prior to analysis ultimately means a fraction of the sample needs to be taken from the bags, although volumes as low as 2 μL suffice, reducing considerably the risk of exposure for personnel. Although Fourier transform infrared instruments are highly robust and reliable in terms of alignment and calibration, requiring minimal maintenance, the technique mainly suffers from the lack of dedicated design for clinical transfer. Nevertheless, recent advancements in the field of ATR-FTIR spectroscopy could help to strengthen the potential of and interest in the technique. For instance, high throughput ATR plates reader (Pike technologies) have been developed to increase the workflow, but also to enable preparation of samples remote from the system. This is of great interest for example to perform sample deposition inside a fume hood and then manipulation of dry samples with reduced hazard. Moreover, a new generation of 3D printed disposable ATR substrates have been developed for single use (64), which could be also adapted for toxic samples. Commercialised by ClinSpec Dx (https://www.clinspecdx.com/), such innovations in the concept of ATR-FTIR spectroscopy could strengthen its position for applications in AQC of chemotherapeutic solutions in clinical settings. Moreover, the brighter light sources of quantum cascade lasers (QCL) could provide increased sensitivity for the emerging alternative of QCL- IR spectroscopy (65). In the near future, infrared spectroscopy could therefore potentially compete with Raman for liquid samples analysis.

5. Conclusion

Analytical quality control of intravenous chemotherapeutic solutions is a critical checkpoint in the process of patient treatment. While chromatography-based gold standards are well established, there is a need to evolve towards rapid and cost-effective methods. Raman and infrared spectroscopy provide label free molecular characterisation of samples in spectral signatures encompassing both quantitative and qualitative information. Despite the contribution from the matrix used to prepare the solutions (either NaCl 0.9% or glucose 5%) or excipients found in the commercial formulas, both techniques deliver accurate identification of the active, and quantification of its concentration. While ultimately Raman spectroscopy could be applied non-invasively, directly into infusion bags, infrared spectroscopy remains a robust and reliable analytical tool for pharmaceuticals characterisation, including chemotherapeutic solutions. Optimisation of methods could lead to user friendly tools supporting fast implantation in the hospital routine.

Acknowledgement

We acknowledge ministry of higher education in Sudan and Campus France for financial support and administrative arrangement of Alaa A. Makki's PhD in cotutelle between the university of Gezira and university of Tours.

References:

1. Nussbaumer S, Bonnabry P, Veuthey JL, Fleury-Souverain S. Analysis of anticancer drugs: A review. Talanta. 2011;85(5):2265–89.
2. Aga QAAK, Bataineh YA, Sbaih HM. Therapeutic drug monitoring of cytotoxic drugs. Int J Drug Deliv Technol [Internet]. 2020;10(2):284–91. Available from: http://ovidsp.ovid.com/ovidweb.cgi?T=JS%7B&%7DPAGE=reference%7B&%7DD=emed5%7B&%7DNEWS=N%7B&%7DAN=2001313284
3. Nardella F, Beck M, Collart-Dutilleul P, Becker G, Boulanger C, Perello L, et al. A UV-Raman spectrometry method for quality control of anticancer preparations: Results after 18 months of implementation in hospital pharmacy. Int J Pharm [Internet]. 2016;499(1–2):343–50. Available from: http://dx.doi.org/10.1016/j.ijpharm.2016.01.002
4. Delmas A, Gordien JB, Bernadou JM, Roudaut M, Gresser A, Malki L, et al. Quantitative and qualitative control of cytotoxic preparations by HPLC-UV in a

centralized parenteral preparations unit. J Pharm Biomed Anal. 2009;49(5):1213–20.
5. Castagne V, Habert H, Abbara C, Rudant E, Bonhomme-Faivre L. Cytotoxics compounded sterile preparation control by HPLC during a 16-month assessment in a French university hospital: Importance of the mixing bags step. J Oncol Pharm Pract. 2011;17(3):191–6.
6. Bondarenko P V., Second TP, Zabrouskov V, Makarov AA, Zhang Z. Mass Measurement and Top-Down HPLC/MS Analysis of Intact Monoclonal Antibodies on a Hybrid Linear Quadrupole Ion Trap-Orbitrap Mass Spectrometer. J Am Soc Mass Spectrom. 2009;20(8):1415–24.
7. Prideaux B, Stoeckli M. Mass spectrometry imaging for drug distribution studies. J Proteomics [Internet]. 2012;75(16):4999–5013. Available from: http://dx.doi.org/10.1016/j.jprot.2012.07.028
8. Osawa T, Naito T, Suzuki N, Imai K, Nakanishi K, Kawakami J. Validated method using liquid chromatography-electrospray ionization tandem mass spectrometry for the determination of contamination of the exterior surface of vials containing platinum anticancer drugs. Talanta. 2011;85(3):1614–20.
9. Kort A, Hillebrand MJX, Cirkel GA, Voest EE, Schinkel AH, Rosing H, et al. Quantification of cabazitaxel, its metabolite docetaxel and the determination of the demethylated metabolites RPR112698 and RPR123142 as docetaxel equivalents in human plasma by liquid chromatography-tandem mass spectrometry. J Chromatogr B Anal Technol Biomed Life Sci [Internet]. 2013;925:117–23. Available from: http://dx.doi.org/10.1016/j.jchromb.2013.02.034
10. Balan V, Mihai CT, Cojocaru FD, Uritu CM, Dodi G, Botezat D, et al. Vibrational spectroscopy fingerprinting in medicine: From molecular to clinical practice. Materials (Basel). 2019;12(18):1–40.
11. Pudlas M, Koch S, Bolwien C, Walles H. Raman spectroscopy as a tool for quality and sterility analysis for tissue engineering applications like cartilage transplants. Int J Artif Organs. 2010;33(4):228–37.
12. Amin A, Bourget P, Vidal F, Ader F. Routine application of Raman spectroscopy in the quality control of hospital compounded ganciclovir. Int J Pharm [Internet]. 2014;474(1–2):193–201. Available from: http://dx.doi.org/10.1016/j.ijpharm.2014.08.028
13. Bourget P, Amin A, Vidal F, Merlette C, Troude P, Baillet-Guffroy A. The contribution of Raman spectroscopy to the analytical quality control of cytotoxic drugs

in a hospital environment: Eliminating the exposure risks for staff members and their work environment. Int J Pharm [Internet]. 2014;470(1–2):70–6. Available from: http://dx.doi.org/10.1016/j.ijpharm.2014.04.064

14. Bourget P, Amin A, Vidal F, Merlette C, Lagarce F. Comparison of Raman spectroscopy vs. high performance liquid chromatography for quality control of complex therapeutic objects: Model of elastomeric portable pumps filled with a fluorouracil solution. J Pharm Biomed Anal [Internet]. 2014;91:176–84. Available from: http://dx.doi.org/10.1016/j.jpba.2013.12.030
15. Lê L, Berge M, Tfayli A, Baillet Guffroy A, Prognon P, Dowek A, et al. Quantification of gemcitabine intravenous drugs by direct measurement in chemotherapy plastic bags using a handheld Raman spectrometer. Talanta. 2019;196:376–80.
16. Solís-Gómez A, Sato-Berrú RY, Mata-Zamora ME, Saniger JM, Guirado-López RA. Characterizing the properties of anticancer silibinin and silybin B complexes with UV–Vis, FT-IR, and Raman spectroscopies: A combined experimental and theoretical study. J Mol Struct. 2019;1182:109–18.
17. Bazin C, Cassard B, Caudron E, Prognon P, Havard L. Comparative analysis of methods for real-time analytical control of chemotherapies preparations. Int J Pharm [Internet]. 2015;494(1):329–36. Available from: http://dx.doi.org/10.1016/j.ijpharm.2015.08.041
18. Bazin C, Vieillard V, Astier A, Paul M. Implementation of real-time identification analysis and quantification of chemotherapies preparations with a Multispec® analyser. Ann Pharm Fr [Internet]. 2014;72(1):33–40. Available from: http://dx.doi.org/10.1016/j.pharma.2013.09.006
19. Bellisola G, Sorio C. Infrared spectroscopy and microscopy in cancer research and diagnosis. Am J Cancer Res. 2012;2(1):1–21.
20. Dziopa F, Galy G, Bauler S, Vincent B, Crochon S, Tall ML, et al. A quantitative and qualitative method to control chemotherapeutic preparations by Fourier transform infrared-ultraviolet spectrophotometry. J Oncol Pharm Pract. 2013;19(2):121–9.
21. Lê LMM, Tfayli A, Zhou J, Prognon P, Baillet-Guffroy A, Caudron E. Discrimination and quantification of two isomeric antineoplastic drugs by rapid and non-invasive analytical control using a handheld Raman spectrometer. Talanta. 2016;161:320–4.
22. Lê L, Berge M, Tfayli A, Prognon P, Caudron E. Discriminative and Quantitative Analysis of Antineoplastic Taxane Drugs Using a Handheld Raman Spectrometer.

Biomed Res Int. 2018;2018:12–5.

23. Lê LMM, Berge M, Tfayli A, Zhou J, Prognon P, Baillet-Guffroy A, et al. Rapid discrimination and quantification analysis of five antineoplastic drugs in aqueous solutions using Raman spectroscopy. Eur J Pharm Sci [Internet]. 2018;111:158–66. Available from: http://dx.doi.org/10.1016/j.ejps.2017.09.046
24. Makki AA, Bonnier F, Respaud R, Chtara F, Tfayli A, Tauber C, et al. Qualitative and quantitative analysis of therapeutic solutions using Raman and infrared spectroscopy. Spectrochim Acta - Part A Mol Biomol Spectrosc. 2019;218:97–108.
25. Bourget P, Amin A, Vidal F, Merlette C, Lagarce F. Comparison of Raman spectroscopy vs. high performance liquid chromatography for quality control of complex therapeutic objects: Model of elastomeric portable pumps filled with a fluorouracil solution. J Pharm Biomed Anal. 2014;91:176–84.
26. Lê LMM, Caudron E, Baillet-Guffroy A, Eveleigh L. Non-invasive quantification of 5 fluorouracil and gemcitabine in aqueous matrix by direct measurement through glass vials using near-infrared spectroscopy. Talanta [Internet]. 2014;119:361–6. Available from: http://dx.doi.org/10.1016/j.talanta.2013.10.060
27. Szuławska A, Czyz M. Molekularne mechanizmy działania antracyklin. Postepy Hig Med Dosw. 2006;60:78–100.
28. Wall R, McMahon G, Crown J, Clynes M, O'Connor R. Rapid and sensitive liquid chromatography-tandem mass spectrometry for the quantitation of epirubicin and identification of metabolites in biological samples. Talanta. 2007;72(1):145–54.
29. Barker IK, Crawford SM, Fell AF. Determination of plasma concentrations of epirubicin and its metabolites by high-performance liquid chromatography during a 96-h infusion in cancer chemotherapy. J Chromatogr B Biomed Appl. 1996;681(2):323–9.
30. Lachâtre F, Marquet P, Ragot S, Gaulier JM, Cardot P, Dupuy JL. Simultaneous determination of four anthracyclines and three metabolites in human serum by liquid chromatography-electrospray mass spectrometry. J Chromatogr B Biomed Sci Appl. 2000;738(2):281–91.
31. Česen M, Kosjek T, Busetti F, Kompare B, Heath E. Human metabolites and transformation products of cyclophosphamide and ifosfamide: analysis, occurrence and formation during abiotic treatments. Environ Sci Pollut Res. 2016;23(11):11209–23.
32. Whelan J, Khan A, Sharma A, Rothermundt C, Dileo P, Michelagnoli M, et al. Interval

compressed vincristine, doxorubicin, cyclophosphamide alternating with ifosfamide, etoposide in patients with advanced Ewing's and other Small Round Cell Sarcomas. Clin Sarcoma Res [Internet]. 2012;2(1):12. Available from: http://www.ncbi.nlm.nih.gov/pubmed/22998944

33. Hagner N, Joerger M. Cancer chemotherapy: Targeting folic acid synthesis. Cancer Manag Res [Internet]. 2010;2(1):293–301. Available from: www.dovepress.com
34. Guardiola E, Peyrade F, Chaigneau L, Cupissol D, Tchiknavorian X, Bompas E, et al. Results of a randomised phase II study comparing docetaxel with methotrexate in patients with recurrent head and neck cancer. Eur J Cancer. 2004;40(14):2071–6.
35. Society MM. , m.d., p. 1995;332(14):1–6.
36. Kantarjian H, Thomas D, O'Brien S, Cortes J, Giles F, Jeha S, et al. Long-term follow-up results of hyperfractionated cyclophosphamide, vincristine, doxorubicin, and dexamethasone (Hyper-CVAD), a dose-intensive regimen, in adult acute lymphocytic leukemia. Cancer. 2004;101(12):2788–801.
37. Ferreri AJM, Reni M, Dell'Oro S, Ciceri F, Bernardi M, Camba L, et al. Combined treatment with high-dose methotrexate, vincristine and procarbazine, without intrathecal chemotherapy, followed by consolidation radiotherapy for primary central nervous system lymphoma in immunocompetent patients. Oncology. 2001;60(2):134–40.
38. Santos Panero P dos, Santos Panero F dos, Santos Panero J dos, Bezerra da Silva HE. Application of Extended Multiplicative Signal Correction to Short-Wavelength near Infrared Spectra of Moisture in Marzipan. J Data Anal Inf Process. 2013;01(03):30–4.
39. Li Q, Gao Q, Zhang G. Improved extended multiplicative scatter correction algorithm applied in blood glucose noninvasive measurement with FT-IR spectroscopy. J Spectrosc. 2013;1(1).
40. Parachalil DR, Bruno C, Bonnier F, Blasco H, Chourpa I, McIntyre J, et al. Raman spectroscopic screening of high and low molecular weight fractions of human serum. Analyst. 2019;144(14):4295–311.
41. Schulze HG, Rangan S, Piret JM, Blades MW, Turner RFB. Developing Fully Automated Quality Control Methods for Preprocessing Raman Spectra of Biomedical and Biological Samples. Appl Spectrosc. 2018;72(9):1322–40.
42. Leger MN, Ryder AG. Comparison of derivative preprocessing and automated polynomial baseline correction method for classification and quantification of narcotics in solid mixtures. Appl Spectrosc. 2006;60(2):182–93.

43. Liland KH, Almøy T, Mevik BH. Optimal choice of baseline correction for multivariate calibration of spectra. Appl Spectrosc. 2010;64(9):1007–16.
44. Vergote GJ, Vervaet C, Remon JP, Haemers T, Verpoort F. Near-infrared FT-Raman spectroscopy as a rapid analytical tool for the determination of diltiazem hydrochloride in tablets. Eur J Pharm Sci. 2002;16(1–2):63–7.
45. Afseth NK, Kohler A. Extended multiplicative signal correction in vibrational spectroscopy, a tutorial. Chemom Intell Lab Syst [Internet]. 2012;117:92–9. Available from: http://dx.doi.org/10.1016/j.chemolab.2012.03.004
46. Chevallier S, Bertrand D, Kohler A, Courcoux P. Application of PLS-DA in multivariate image analysis. J Chemom. 2006;20(5):221–9.
47. Bonnier F, Byrne HJ. Understanding the molecular information contained in principal component analysis of vibrational spectra of biological systems. Analyst. 2012;137(2):322–32.
48. Lee LC, Liong CY, Jemain AA. Partial least squares-discriminant analysis (PLS-DA) for classification of high-dimensional (HD) data: A review of contemporary practice strategies and knowledge gaps. Analyst. 2018;143(15):3526–39.
49. Szafraniec E, Majzner K, Farhane Z, Byrne HJ, Lukawska M, Oszczapowicz I, et al. Spectroscopic studies of anthracyclines: Structural characterization and in vitro tracking. Spectrochim Acta - Part A Mol Biomol Spectrosc [Internet]. 2016;169:152–60. Available from: http://dx.doi.org/10.1016/j.saa.2016.06.035
50. Sottani C, Tranfo G, Bettinelli M, Faranda P, Spagnoli M, Minoia C. Trace determination of anthracyclines in urine: A new high-performance liquid chromatography/tandem mass spectrometry method for assessing exposure of hospital personnel. Rapid Commun Mass Spectrom. 2004;18(20):2426–36.
51. Ricciarello R, Pichini S, Pacifici R, Altieri I, Pellegrini M, Fattorossi A, et al. Simultaneous determination of epirubicin, doxorubicin and their principal metabolites in human plasma by high-performance liquid chromatography and electrochemical detection. J Chromatogr B Biomed Appl. 1998;707(1–2):219–25.
52. Martins I, Souza JO, Sanson AL, Vieira EP, Giusti-Paiva A. Simultaneous determination of cyclophosphamide and ifosfamide in plasma using SPEHPLC-UV method. Lat Am J Pharm. 2009;28(1):41–6.
53. Lê LMM, Berge M, Tfayli A, Zhou J, Prognon P, Baillet-Guffroy A, et al. Rapid discrimination and quantification analysis of five antineoplastic drugs in aqueous solutions using Raman spectroscopy. Eur J Pharm Sci. 2018;111:158–66.

54. Badawi HM, Förner W. DFT and MP2 study of the molecular structure and vibrational spectra of the anticancer agent cyclophosphamide. Zeitschrift fur Naturforsch - Sect B J Chem Sci. 2012;67(12):1305–13.
55. Ayyappan S, Sundaraganesan N, Aroulmoji V, Murano E, Sebastian S. Molecular structure, vibrational spectra and DFT molecular orbital calculations (TD-DFT and NMR) of the antiproliferative drug Methotrexate. Spectrochim Acta - Part A Mol Biomol Spectrosc. 2010;77(1):264–75.
56. Mourant JR, Johnson TM, Los G, Bigio IJ. Non-invasive measurement of chemotherapy drug concentrations in tissue: Preliminary demonstrations of in vivo measurements. Phys Med Biol. 1999;44(5):1397–417.
57. Bonnier F, Brachet G, Duong R, Sojinrin T, Respaud R, Aubrey N, et al. Screening the low molecular weight fraction of human serum using ATR-IR spectroscopy. J Biophotonics. 2016;9(10):1085–97.
58. Matousek P. Deep non-invasive Raman spectroscopy of living tissue and powders. Chem Soc Rev. 2007;36(8):1292–304.
59. Movasaghi Z, Rehman S, Rehman IU. Raman spectroscopy of biological tissues. Appl Spectrosc Rev. 2007;42(5):493–541.
60. Paudel A, Raijada D, Rantanen J. Raman spectroscopy in pharmaceutical product design. Adv Drug Deliv Rev [Internet]. 2015;89:3–20. Available from: http://dx.doi.org/10.1016/j.addr.2015.04.003
61. Ellis DI, Cowcher DP, Ashton L, O'Hagan S, Goodacre R. Illuminating disease and enlightening biomedicine: Raman spectroscopy as a diagnostic tool. Analyst. 2013;138(14):3871–84.
62. Eliasson C, Matousek P. Noninvasive authentication of pharmaceutical products through packaging using spatially offset Raman spectroscopy. Anal Chem. 2007;79(4):1696–701.
63. Yang H, Yang S, Kong J, Dong A, Yu S. Obtaining information about protein secondary structures in aqueous solution using Fourier transform IR spectroscopy. Nat Protoc. 2015;10(3):382–96.
64. Butler HJ, Brennan PM, Cameron JM, Finlayson D, Hegarty MG, Jenkinson MD, et al. Development of high-throughput ATR-FTIR technology for rapid triage of brain cancer. Nat Commun [Internet]. 2019;10(1):1–9. Available from: http://dx.doi.org/10.1038/s41467-019-12527-5
65. Sala A, Spalding KE, Ashton KM, Board R, Butler HJ, Dawson TP, et al. Rapid

analysis of disease state in liquid human serum combining infrared spectroscopy and “digital drying.” J Biophotonics. 2020;13(9):1–10.